Quantum Dots for Multimodal Bioimaging and Sensing Applications

Swadeshmukul Santra,[1] Heesun Yang[2], Soumitra Kar,[3] Subir K. Sabui[3], Parvesh Sharma[4], Paul H. Holloway[5], Glenn A. Walter[6], Brij M. Moudgil[4], and Edward Scott[7]

[1]NanoScience Technology Center, Department of Chemistry and Biomolecular Science Center, University of Central Florida, Orlando, FL 32826, USA
Fax: 1 407 882 2819; Tel: 1 407 882 2848
ssantra@mail.ucf.edu
[2]Department of Materials Science and Engineering, Hongik University, Seoul, 121-791, Korea
[3]NanoScience Technology Center, University of Central Florida, Orlando, FL 32826, USA
[4]Particle Engineering Research Center and Material Science and Engineering, University of Florida, Gainesville, 32611, USA
[5]Department of Materials Science and Engineering, University of Florida, Gainesville, 32611, USA
[6]Department of Physiology and Functional Genomics, McKnight Brain Institute, University of Florida, Gainesville, FL 32611, USA
[7]Department of Molecular Genetics and Microbiology, University of Florida, Gainesville, 32611, USA

ABSTRACT

Fluorescent quantum dots (Qdots) have demonstrated their potential in diagnostic bioimaging applications in vitro. For in vivo bioimaging applications, however, the embodiment of additional properties such as paramagnetism onto the same fluorescent probes is highly desirable. These multimodal probes would benefit in vivo disease diagnosis and surgical guidance based on their ability to be detected in multiple modes (i.e. optically and magnetically). A single-step multimodal Qdot synthesis and surface modification technique that can be used for making various engineered multimodal nanoparticles including Qdots is described here. The development of paramagnetic Gd^{III}-functionalized fluorescent Qdots and their applications in labeling various biological entities such as cells and tissues will be demonstrated.

1. INTRODUCTION

More than a decade-long studies on colloidal luminescent quantum dots (Qdots) have revealed that the effective surface passivation is critical in making Qdots extremely bright and photostable[1-7]. A robust surface passivation will thus produce high quality Qdots [7-15]. Over the past several years, fluorescent quantum dots (Qdots) have been well studied and have shown tremendous potential in labeling biological entities such as cells, tissues and biohazard particles (bacteria, viruses, etc.). Qdots stand out from conventional organic based dyes in at least two aspects: photostability and sensitivity. Due to their hydrophobic surface property, an appropriate surface coating is necessary to disperse Qdots in aqueous solution. Coating also protects them from photo-initiated surface degradation, which is directly related to fading of fluorescence intensity and toxicity. Despite recently reported toxic effects of quantum dots, both *in vitro* and *in vivo* studies have been reported in favor of using Qdots for biolabeling applications, including *in vivo* disease diagnosis.

2. EXPERIMENTAL SECTION

Qdots were synthesized using AOT/heptane/water microemulsion system. Typically, $Cd(CH_3COO)_2.2H_2O$, $Mn(CH_3COO)_2$, Na_2S, and $Zn(CH_3COO)_2$ were used for the preparation of (Cd^{2+} + Mn^{2+})-, S^{2-}-, and Zn^{2+}-containing the standard aqueous solutions. Each aqueous solution was stirred with an AOT/heptane solution, forming the micellar solution. Mn doped CdS core nanocrystals were formed by mixing (Cd^{2+} + Mn^{2+})- and S^{2-}-containing micellar solutions rapidly for 10-15 min. The W_0 value for the W/O microemulsion was 10 and the total microemulsion volume was 87 ml. For the growth of a shell layer, a Zn^{2+}-containing micellar solution was added at a very slow rate (1.5 ml/min) into the CdS:Mn nanocrystal micellar solution. The nucleation and growth of a separate ZnS phase were suppressed by the very slow addition of the Zn^{2+}-containing micellar solution.

After addition of the Zn^{2+}-containing microemulsion, 7.4 mL of tetraethyl orthosilicate (TEOS) was injected into the CdS:Mn/ZnS core/shell Qdot microemulsion and mixed for 15 min at room temperature. The hydrolysis and condensation reactions were initiated by adding NH_4OH in the form of a microemulsion, which is

prepared by mixing 4.44 mL of NH_4OH (30 wt%) with a AOT (11 g)/heptane (150 mL) solution. After condensation for 24 hr at room temperature, 3.7 mL of TEOS and 0.74 mL of 3-(aminopropyl) triethoxysilane (APTS) were injected into the above solution and mixed for 15 min. Subsequently, NH_4OH microemulsion (prepared by mixing 2.64 mL of NH_4OH with AOT (6.54 g)/heptane (50 mL) solution) was injected. Another microemulsion, prepared by mixing 2.22 mL of 3-(trihydroxysilyl) propyl methylphosphonate (THPMP) plus 1.11 mL of *n*-(trimethoxysilylpropyl)ethyldiamine, triacetic acid trisodium salt (TSPETE) in 10.66 mL of water with AOT (13.09 g)/heptane (50 mL) solution, was injected and reacted for 24 hr. A Gd^{3+} microemulsion (prepared by mixing 0.3608 g of Gd acetate in 5.28 mL of water with AOT (13.09 g)/heptane (50 mL)) was injected and reacted for 24 hr. These functionalized Qdots were precipitated by addition of a small amount of methanol, followed by a thorough washing with methanol. The Gd-Qdots were dispersed and stable in a phosphate buffer saline solution (pH 7.4).

3. RESULTS AND DISCUSSIONS

Figure 1 shows the bright yellow color of the quantum dots. The digital image of the qThe QDs were characterized by transmission electron microscopy to measure the particle size both before and after their surface coating with the silica layer. The average particle size of the as synthesized CdS:Mn/ZnS core/shell quantum dots was estimated to be ~ 3nm. Figure 2 exhibits overlapped silica-coated quantum dots, the contrast between the light gray amorphous silica layer (4−7 nm thick) and the dark CdS:Mn/ZnS quantum dot (~3 nm in diameter) is apparent [16]. The room temperature

Figure 1. Bright yellow emission from the QDs

photoluminescence measurements (see Fig. 3) exhibited a bright yellow emission band at 590 nm attributed to the Mn impurities [17]. The excitation and decay of the Mn^{2+} ions produces a yellow luminescence at approximately 590 nm associated with a transition between $^4T_1$ and $^6A_1$ energy levels.

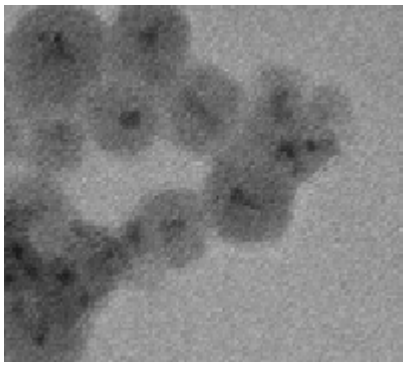

Figure 2. TEM image of the silica coated QDs

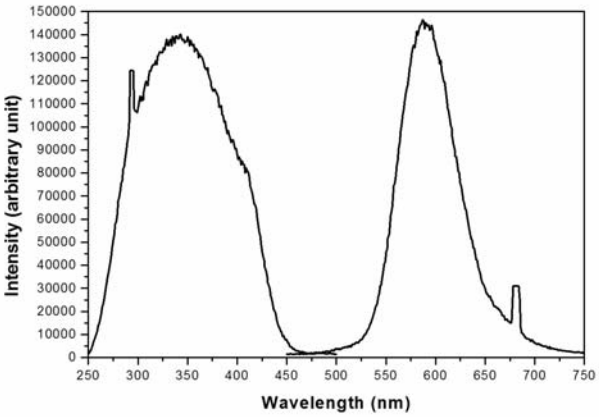

Figure 3. Fluorescence excitation (monitored at 590 nm) and emission (excited at 345 nm) spectra of Gd-Qdots

X-ray photoelectron spectroscopic (XPS) studies were carried out to demonstrate that Gd^{III} was present on the quantum dot surface. The Cd $3d_{5/2}$, Zn $2p_{3/2}$, and Si 2p photoelectron peaks were detected from the CdS core, ZnS shell, and SiO_2 layer, respectively. The S 2s and 2p peaks were rarely detected in the spectra because they have low sensitivity factors compared to other elements, and they are presumably buried by the relatively thick SiO_2 coating. The Gd 3d peak at ~1191 eV is easily detected, indicating that TSPETE is an efficient silane agent for capture of Gd^{III} ions. Using inductively coupled plasma (ICP) analysis, the number of Gd^{III} ions per particle was determined to be approximately 107. For comparison, the number of Gd ions in the synthetic polymer-based (i.e., polylysine or its derivatives) and dendrimer-based Gd^{III} chelate contrast agents were reported to range from 6−70 and 5−1331,

NSTI-Nanotech 2007, www.nsti.org, ISBN 1420061836 Vol. 2, 2007

respectively, depending strongly on the dimensions of the macromolecules [18]. The schematic model of the multimodal QDS is shown in Fig. 4.

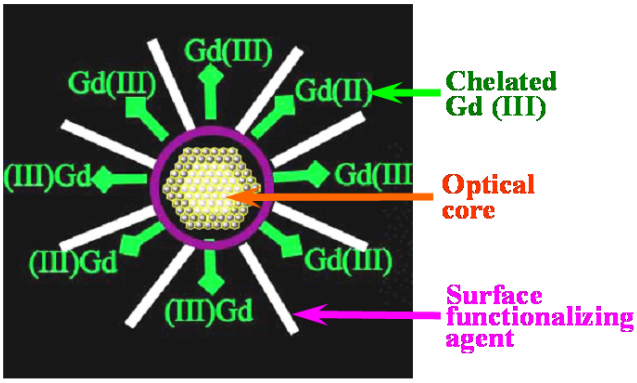

Figure 4. Schematic representation of the multimodal quantum dots.

Longitudinal (T_1) and transverse proton relaxation time (T_2)-were determined as a function of Gd-Qdots concentration at 4.7 T (Tesla). Increased MR signal intensity is observed with increasing Gd concentrations due to the shorter water T_1. On T_2-weighted images (TR=11000 ms, TE=24 ms), MR image signal intensity is substantially decreased by the effect of increased Gd on water T_2. For control experiments, T_1- and T_2-weighted images of serial dilutions of Qdots without Gd^{III} ions were recorded (not shown here) and could not be distinguished from those of DI water only. The efficacy of a contrast agent is generally expressed by its relaxivity (R_i, i=1, 2), that is defined as the gradient of the linear plot of relaxation rates ($1/T_i$, i=1, 2) versus Gd concentration [Gd],[16] i.e., $1/T_i = 1/T^o + R_i[\mathrm{Gd}]$, where T_i is the relaxation time for a contrast agent solution concentration [Gd], and T^o is the relaxation time in the absence of a contrast agent. From the studies the relaxivities R_1 and R_2 are determined to be 20.5 and 151 $mM^{-1}s^{-1}$, respectively. When compared with commercially available contrast agents, Gd-Qdots exhibit much higher R_1 and R_2 values under the same magnetic strength of 4.7 T [19]. As a direct comparison we determined the proton relaxivities for a commercially available gadoteridol and found it possessed a R_1 of 5.8 $mM^{-1}s^{-1}$ and a R_2 of 7.4 $mM^{-1}s^{-1}$ when measured under exactly the same experimental conditions as the Gd-Qdots. The relaxivity of a contrast agent depends on a number of molecular factors but is normally dominated by the tumbling rate, the water exchange rate, and the availability of water coordination [19]. High relaxivities have been achieved by slowing the tumbling rate of Gd^{III}-based contrast agents (i.e., Gd-DTPA) by grafting the contrast agent to rigid macromolecules and avoiding free rotation of the chelate [19]. In the present case, it is reasonable to speculate that Gd^{III}-coordinated TSPETE is strongly anchored by the rigid silica-coated quantum dots, resulting a low tumbling rate and subsequently high relaxivity. Although there are five Gd^{III} coordination sites on TSPEPE, the possibility that Gd^{III} ions are further coordinated by adjacent silanol ($Si{-}O^-$) or terminal groups from APTS and THPMP can not be eliminated. Therefore, it is unclear as to whether or not the availability of the paramagnetic centers for the access of water molecules affects the relaxivity of Gd-Qdots. Further studies of the structural environments around the Gd centers are underway. It is noted that it is preferable for T_1 contrast agents to have R_2/R_1 ratios of 1–2, while agents used for the T_2 contrast have ratios greater than 10 [16]. Although the present Gd-Qdots can serve as either T_1 or T_2 contrast agents, the R_2/R_1 ratio of ~7.4 indicates that they may be more effective as a T_2 contrast agent.

Preliminary cell-studies indicated encouraging results as could be seen in Figure 5. The quantum dots could be easily incorporated within the cells and subsequently they could be labeled through the bright emission from the QDs.

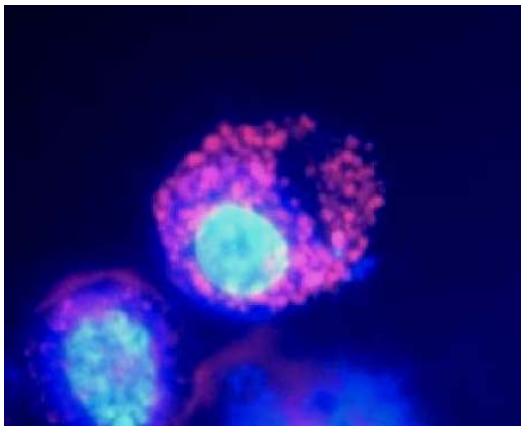

Figure 5. Fluorescence image of QD loaded J 77 murine macrophase (Pink emission from QDs and blue emission from DAPI).

4. CONCLUSIONS

In short, multimodal-imaging quantum dots with an inner crystal diameter of ~ 3 nm and a 4–7 nm thick silica layer have been developed. Paramagnetic Gd^{III} functionalization via a metalchelating silane coupling agent (TSPETE) to the yellow fluorescent, silica-coated CdS:Mn/ZnS core/shell quantum dots resulted in multimodal nanoparticles that can be imaged optically and by MRI. An average of 107 Gd^{III} ions per quantum dot was attached. Gd–Qdots possessed large proton relaxivities of 20.5 $mM^{-1}s^{-1}$ ($R1$) and 151 $mM^{-1}s^{-1}$ ($R2$) and are a promising MRI contrast agent that could be used for biological imaging of live cells.

ACKNOWLEDGEMENT

The authors acknowledge the financial support of the National Science Foundation (NSF Grant EEC-94-02989 and NSF-NIRT Grant EEC-056560).

REFERENCE

(1) Alivisatos, A. P. *Science* **1996**, *271*, 933-937.
(2) Alivisatos, P. *Nature Biotechnology* **2004**, *22*, 47-52.
(3) Bruchez, M.; Moronne, M.; Gin, P.; Weiss, S.; Alivisatos, A. P. *Science* **1998**, *281*, 2013-2016.
(4) Chan, W. C. W.; Nie, S. *Science* **1998**, *281*, 2016-2018.
(5) Medintz, I. L.; Uyeda, H. T.; Goldman, E. R.; Mattoussi, H. *Nature Materials* **2005**, *4*, 435-446.
(6) Michalet, X.; Pinaud, F. F.; Bentolila, L. A.; Tsay, J. M.; Doose, S.; Li, J. J.; Sundaresan, G.; Wu, A. M.; Gambhir, S. S.; Weiss, S. *Science* **2005**, *307*, 538-544.
(7) Peng, X.; Schlamp, M. C.; Kadavanich, A. V.; Alivisatos, A. P. *Journal of the American Chemical Society* **1997**, *119*, 7019-7029.
(8) Hines, M. A.; Guyot-Sionnest, P. *Journal of Physical Chemistry* **1996**, *100*, 468-471.
(9) Dabbousi, B. O.; RodriguezViejo, J.; Mikulec, F. V.; Heine, J. R.; Mattoussi, H.; Ober, R.; Jensen, K. F.; Bawendi, M. G. *Journal of Physical Chemistry B* **1997**, *101*, 9463-9475.
(10) Kortan, A. R.; Hull, R.; Opila, R. L.; Bawendi, M. G.; Steigerwald, M. L.; Carroll, P. J.; Brus, L. E. *Journal of the American Chemical Society* **1990**, *112*, 1327-1332.
(11) Tian, Y. C.; Newton, T.; Kotov, N. A.; Guldi, D. M.; Fendler, J. H. *Journal of Physical Chemistry* **1996**, *100*, 8927-8939.
(12) Danek, M.; Jensen, K. F.; Murray, C. B.; Bawendi, M. G. *Chemistry of Materials* **1996**, *8*, 173-180.
(13) Hoener, C. F.; Allan, K. A.; Bard, A. J.; Campion, A.; Fox, M. A.; Mallouk, T. E.; Webber, S. E.; White, J. M. *Journal of Physical Chemistry* **1992**, *96*, 3812-3817.
(14) Song, K.-K.; Lee, S. *Current Applied Physics* **2001**, *1*, 169-173.
(15) Yang, H.; Holloway, P. H. *Advanced Functional Materials* **2004**, *14*, 152-156.
(16) Yang, H.; Santra, S.; Walter, G. A.; Holloway, P. H. *Advanced Materials* **2006**, *18*, 2890-2894.
(17) Santra, S.; Yang, H.; Holloway, P. H.; Stanley, J. T.; Mericle, R. A. *J. Am. Chem. Soc.* **2005,** *127***,** 1656-1657.
(18) P. Caravan, J. J. Ellison, T. J. McMurry, R. B. Lauffer, *Chem. Rev.* **1999**, *99*, 2293.
(19) Tan, W. B.; Zhang, Y. *Adv. Mater.* **2005**, *17*, 2375.